IONOSPHERIC EQUATORIAL SCINTILLATION CHARACTERISTICS

Y. Béniguel, JP. Adam

IEEA, 13, Promenade Paul Doumer, 92400 Courbevoie, France, beniguel@ieea.fr

ABSTRACT

Earth satellite links may be affected by signal scintillations after propagation through ionosphere due to the occurrence of electron density bubbles inside this medium. These signal scintillations affect the navigation systems performance. In order to assess the receiver capabilities to operate in such an environment it is important to characterise these scintillations. This is the object of this paper.

1 INTRODUCTION

The ionosphere signal scintillations mainly occur around the magnetic equator (- 20° to + 20° magnetic latitude) and at polar regions (> 60°). This was first presented in a paper by Aarons in 1982 [1]. The main parameters, as the field statistical moments, up to the fourth order, were detailed in a paper by Yeh and Liu [2].

This topic has been the object of many measurements campaigns mainly in South America [3], [4], India [5] and Japan [6], [7] and more recently under an ESA / ESTEC initiative [8]. Several review papers have been published on this specific topic [9], [10].

In this paper we will review the main characteristics of equatorial scintillations, in particular the spectrum, the probabilities of occurrence and the fades statistics.

2 SIGNAL SPECTRUM

In the following figures a 1 minute sample is used as an example: satellite PRN 2, day 315, year 2006 at Cayenne (Guiana). The normalized power is the power divided by the mean value over the 1 minute. The detrended phase is obtained with a 6th-order high-pass butterworth filter. The cutoff frequency is set to 0.1 Hz. The computed scintillations parameters are: S4 = 0.51 and σphi = 0.11 radian. The computed power spectral density (PSD) is added for the amplitude and for the phase. The effect of the high-pass filter can be observed below 0.1 Hz on the phase PSD.

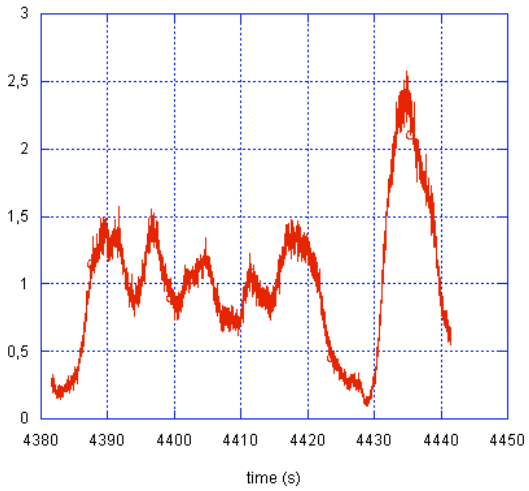

Figure 1: Detrended power

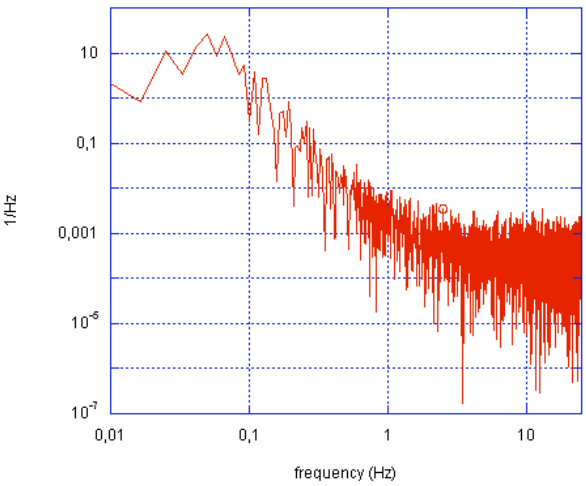

Figure 2: Intensity PSD

The power spectral density has a cut off frequency around 0.1 Hz. It then exhibits a linear slope in a log log axis representation.

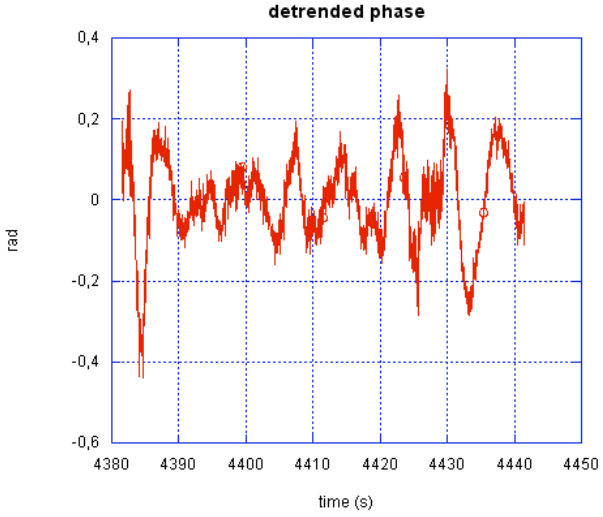

Figure 3: Detrended phase

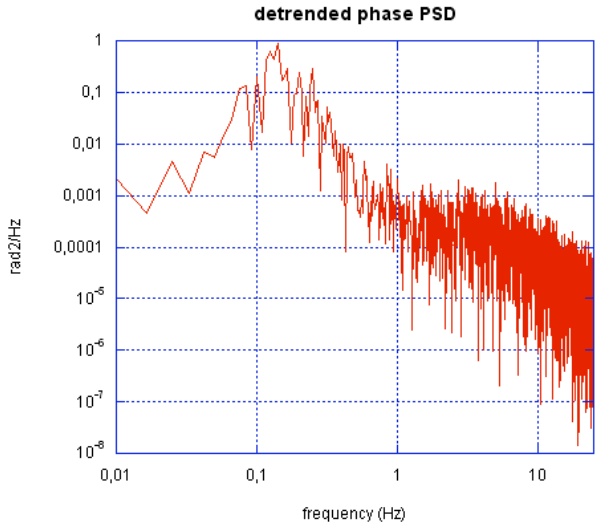

Figure 4: Phase power spectrum

In order to analyze the raw data, the PSD must be synthesized into a small number of parameters. The PSD is usually characterized by its strength at 1 Hz (T) and by its index of power law decay (p). On a log-log representation, these parameters are obtained by fitting a line to the data points using least squares. The frequency range for that linear fit begins at 0.1 Hz, which is the cutoff frequency of the high-pass filter. In order to prevent this fit from extending down into the system noise which biases p towards lower values, the considered frequency range ends at 1 Hz.

This processing is applied to every 1 minute sample of the downloaded RINEX files. Simplified criterions were used for selection of valid samples:

- No missing measurements (3000 points in a 1 minute sample)
- S4 > 0.2 to avoid weak multipath
- σphi < 2. to check the filter convergence

This analysis has been conducted on several days. The considered raw data correspond to days 314 to 318, year 2006 (10/11/2006 to 14/11/2006) in Cayenne. These files were chosen because the computed scintillation parameters have shown significant scintillation activity.

The following figures present the histogram of the p index for the power and the detrended phase PSD. These histograms are directly related to the probability density distributions of p. It can be observed that both distributions are centered on 2.8. Usually, p is considered to be in the range between 1 and 4. In addition, 2.5 is a commonly chosen value for p at equatorial latitudes. The observed distributions are compatible with these statements.

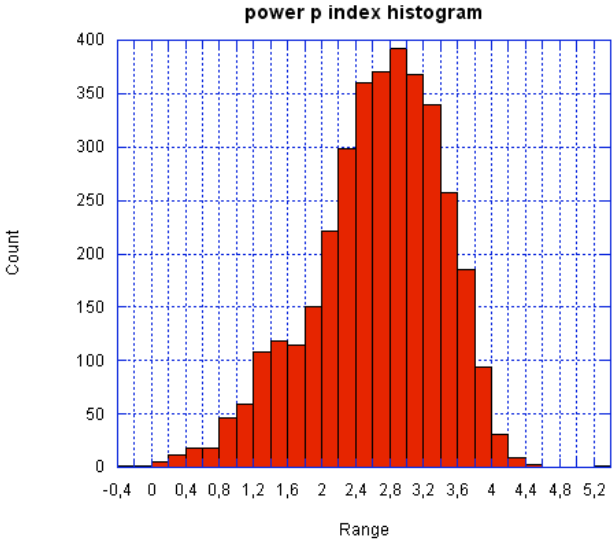

Figure 5: Slope power histogram

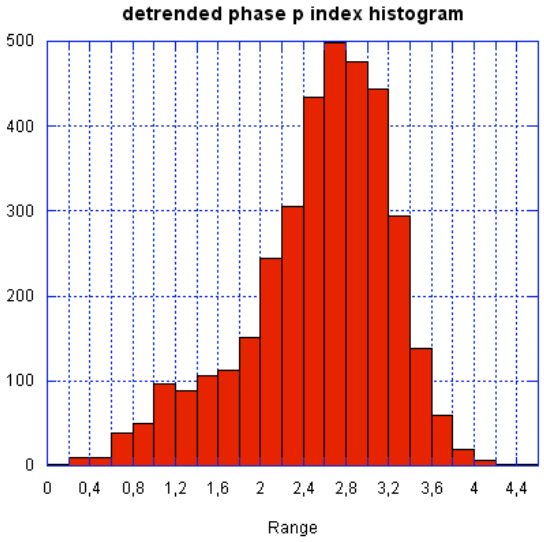

Figure 6: slope phase histogram

The phase PSD can be approximated by Tf^{-p}. As a consequence, the phase standard deviation σphi is expressed as following, where fc is the cutoff frequency :

$$\sigma phi^2 = 2\int_{fc}^{\infty} PSD(f)df = 2\int_{fc}^{\infty} Tf^{-p}df = 2T\left[\frac{f^{-p+1}}{-p+1}\right]_{fc}^{\infty}$$

$$\sigma phi^2 = \frac{2T}{(p-1)\,fc^{p-1}} \qquad (\text{if } p > 1)$$

Since S4 isn't a standard deviation, such a simple relation between S4 and the power PSD is not expected.

The following figure presents σphi computed from the previous equation as a function of the σphi computed as the standard deviation of the time series, for every 1 minute sample. It seems that the two values of σphi are proportional. However, the actual coefficient is different from 1. There may be an omitted factor in the definition of the PSD. Anyway, the correlation between the value deduced from the frequency domain and the value deduced from the time domain is remarkable. This observation and the previous realistic p distribution seem to prove that the extraction of the spectral parameters is reliable.

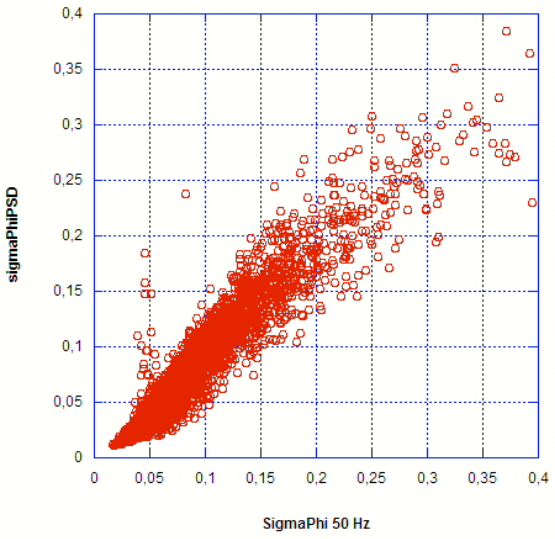

Figure 7: Phase standard deviation: spectrum deduced value vs time series deduced value

3 MODELLING

The scintillation signal has to have an equivalent power spectral density (PSD) given by the relationship:

$$\Gamma = \frac{A}{(q + q_0)^{-p}}$$

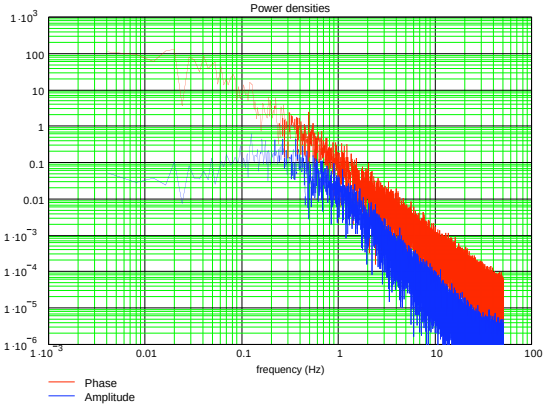

Figure 8: Modelling intensity and phase spectrum

It is determined by three parameters:

- The slope p,
- The cut-off frequency $q_0 = 2\pi / L_0$, where L_0 corresponds to the bubbles correlation distance
- The threshold value A or equivalently the value at 1 Hz

To synthesize the medium irregularities, a value is given to these three parameters in order to calculate the PSD using the formula above, depending on the frequency.

The propagation through this medium is then calculated using the parabolic equation [11]. Time series at receiver level are generated and used for the calculation of the scintillation indices (intensity and phase)

4 PHASE JUMPS

High fluctuating signals lead to deep fades and correlatively to phase jumps as shown on figure 9.

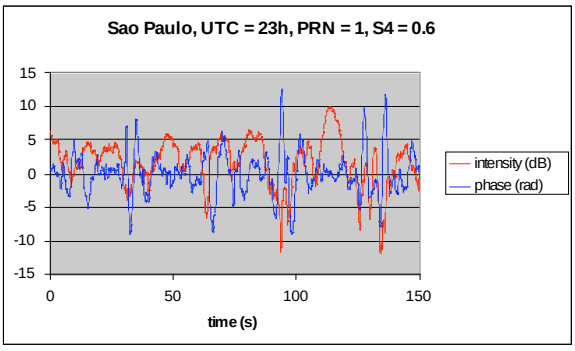

Figure 9: simultaneity occurrence of deep fades and phase peaks

Such an analysis has been made extensively using both the signal and its derivative on GPS signals measurements in Brazil. This is reported on Figures 10 & 11.

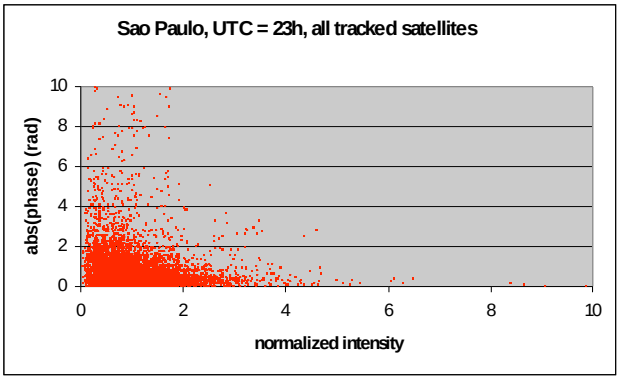

Figure 10 : simultaneous occurrence of deep fades and phase peaks

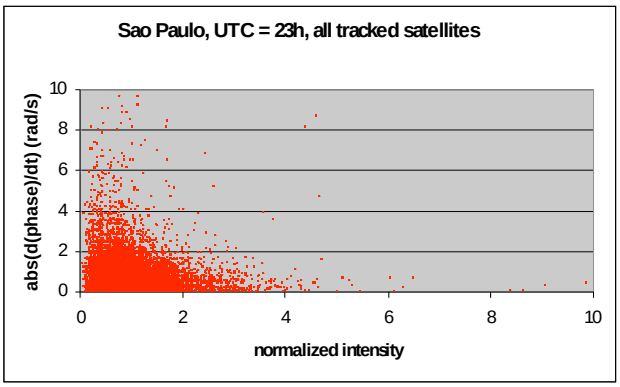

Figure 11: simultaneous occurrence of deep fades and peaks in the phase derivative.

The same behaviour is reproduced with our scintillation model [11]. As far as S4 is lower than a significant value (around 0.7), the phase and intensity standard deviations have correlated values and in the same range. When phase jumps occur, the phase standard deviation increases significantly and S4 and σphi are no more correlated.

5 PROBABILITIES

In order to compute reasonable amplitude and phase distribution, a 10 minutes sample was considered from satellite PRN 13, day 315 in year 2006. The amplitude is the square root of the power. The computed scintillations parameters are S4 = 0.6 and σphi = 0.1. These parameters are use to evaluate the theoretical distributions of the amplitude and the phase: respectively a Nakagami and a gaussian distribution. The following figures present the considered time series and their distributions compared with the theoretical distributions. The obtained distributions are coherent

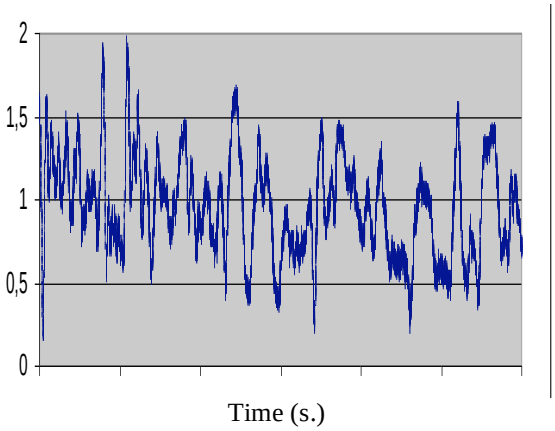

Figure 12 Normalised amplitude

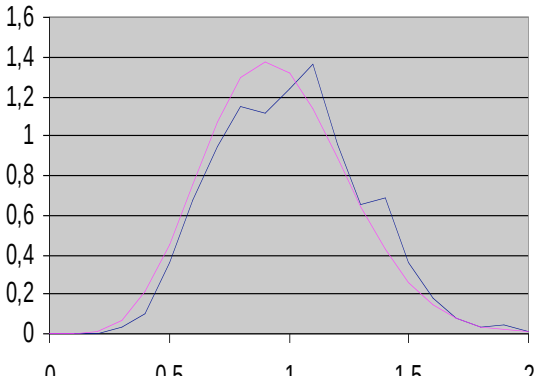

Figure 13 Amplitude distribution measurements (blue) and Nakagami distribution (red)

The comparison between Nakagami distribution and the result obtained using a numerical model is presented on Figure 14.

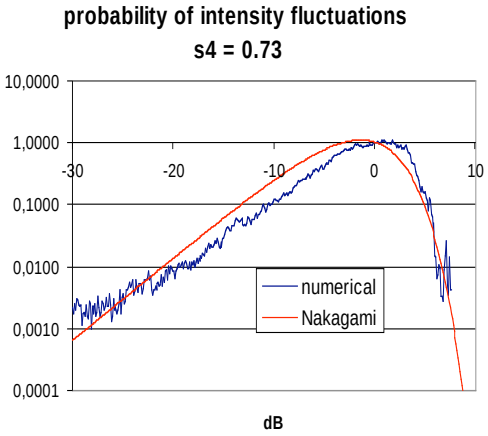

Figure 14 : Comparison between the Nakagami distribution and the one deduced from time series obtained with GISM model.

6 CODE CARRIER DIVERGENCE

The analysis of scintillations implies to get rid of multipath occurrence at beginning and end of the satellite tracks. One way to proceed is to use a code carrier divergence criterion. Based on this criterion, one empirical algorithm has been proposed by A.J. Van Dierendonck [12] which gives quite satisfactory results. The following plot shows the detrended pseudo range and carrier phase on one sample which illustrates this point. It is assumed in the algorithm that there is no code carrier divergence.

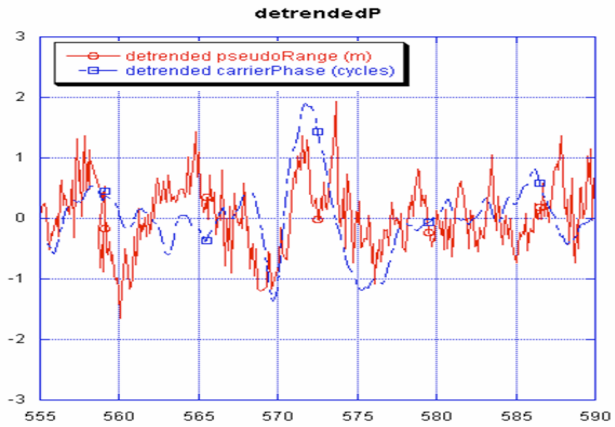

Figure 15: Code carrier divergence

7 CONCLUSION

The characteristics of equatorial scintillations have been presented. The results are mainly deduced from an ESA / ESTEC measurement campaign in year 2006, i.e. corresponding to a low solar activity year. Despite this low solar activity, a number of significant events were measured allowing estimating the scintillation main features.

The spectrum characteristics, namely the slope and the strength, have been estimated from samples recorded during one week with significant events and correspond to what is usually presented in the literature. Also the probabilities have been estimated and compared to the usual global trends.

We have pointed out the problem of phase jumps in the case of very deep fades. This is of particular interest for testing GPS receivers in a strong fluctuating environment. However, additional statistical data would be required in that case for a more precise analysis. These events occur for high values of the scintillation index S4, and not enough samples were corresponding to that case.

8 REFERENCES

[1] Aarons J. Global morphology of ionospheric scintillations, Proc. IEEE, 70 (4), 360 – 378, 1982

[2] Yeh C. K. and C. H. Liu, “Radio wave scintillations in the ionosphere’, Proc. IEEE, Vol. 70, N. 4, pp. 325 – 378, 1982

[3] Doherty, P.H., S.H. Delay, C.E. Valladares, J. Klobuchar, “Ionospheric scintillation effects in the equatorial and auroral regions”, pp. 662 - 671, ION - GPS - 2000, Salt Lake City, Utah, September 19 – 22, 2000

[4] De Paula E., P.H. Doherty, T. Dehel, “Scintillation activity and recent measurements from the Brazilian region”, SBAS – IONO meeting, Maastricht, May 2001

[5] Chandra H., Ramarao P. V. S., Vijay Kumar P. N., Pathan B. M., Iyer K. N., Gwal A. K., Singh R. P., Birbal Singh, Dasgupta A., “VHF scintillations at low latitudes in India”, Beacon Satellite Symposium, Boston College, Boston, 2007

[6] El-Arini, M. B., R. S. Conker, S. D. Ericson, K. W. Bean, F. Niles, K. Matsunaga, and K. Hoshinoo, “Analysis of the Effects of Ionospheric Scintillation on GPS L2 in Japan” ION-GPS-2003, Portland, OR, September 2003

[7] Otsuka, Y., K. Shiokawa, and T. Ogawa, Equatorial ionospheric scintillations and zonal irregularity drifts observed with closely-spaced GPS receivers in Indonesia, *J. Meteorological Soc. Japan*, 84A, 343 – 351, 2006

[8] Béniguel Y., J-P Adam, N. Jakowski, T. Noack, V. Wilken, J-J Valette, M. Cueto, A. Bourdillon, P. Lassudrie-Duchesne, B. Arbesser-Rastburg, 2009, Analysis of scintillation recorded during the PRIS measurement campaign, Radio Sci., 44, doi 1029/2008RS004090

[9] Basu, S. and S. Basu, Equatorial scintillations: Advances since ISEA - 6, J. Atmos Terr Phys, 47, 753 – 768, 1985

[10] Basu, S. et al., “Scintillations, plasma drifts and neutral winds in the equatorial ionosphere after sunset”, Journal of geophysical research, 101 (A12), 26, 795 – 809, 1996

[11] Béniguel Y. 2002, GIM A global ionospheric propagation model for scintillations of transmitted signals”, Radio Sci., 37 (3), 1032, doi 1029/2000RS002393

[12] GSV4004B User Manual GPS Ionospheric Scintillation & TEC monitor